Decoupling Cell and Matrix Mechanics in Engineered Microtissues Using Magnetically Actuated Microcantilevers

Ruogang Zhao, Thomas Boudou, Wei-Gang Wang, Christopher S. Chen, and Daniel H. Reich**

Engineered tissues hold great promise for repairing damaged organs,[1,2] and as model systems for biomaterials research and drug screening.[3] While structural details and biological characteristics have typically been the focus of benchmarking for engineered tissues,[1,2] the importance of their mechanical properties has been recently recognized.[4–6] For example, studies have shown that improved mechanical properties can enhance engineered tissues' biological function.[7–9] The biomechanics of engineered tissue has generally been studied by culturing and mechanically conditioning centimeter-scale tissue constructs and then transferring samples to a conventional testing apparatus for mechanical property evaluation.[8,10,11] While such approaches have significantly advanced understanding of the physical properties of engineered tissues, they suffer from several major limitations including low throughput, high diffusion barriers for soluble factors caused by the large specimen sizes, and perturbations introduced by the sample handling needed to conduct mechanical tests.

The recent emergence of bio-microelectromechanical systems (bio-MEMS) has provided the potential for improved research tools for tissue biomechanics.[12–15] For example, 3D microtissues created in patterned poly(dimethylsiloxane) (PDMS) substrates have allowed fast diffusion of soluble factors to many samples simultaneously,[16,17] and a recently developed microtissue force gauge has enabled measurement of contraction forces in arrays of 3D microtissues.[18,19] However, despite these significant advances, these systems lack a key functional feature that more conventional testing systems offer: the capability to apply external mechanical loading to the samples. The absence of this feature prohibits either mechanical conditioning of the tissues or measurements of tissue stiffness, which greatly limits the utility of such systems in biomechanical studies. We present here a 3D microtissue culture system that integrates the advantages of existing bio-MEMS approaches with the capability of applying external loading to tissue samples via magnetic actuation. This integrated magnetic microtissue tester (MMT) system enables simultaneous quantification of both the tissue contraction force and tissue stiffness, two of the most critical mechanical parameters for the regulation of cellular biological functions.[4–7] Using this culture system, we studied the cell and matrix contributions to the material properties of fibroblast populated collagen microtissues. By uncoupling the contributions by these two constituents in either static or dynamic loading conditions, we found that they play different roles in contributing to the microtissues' mechanical properties under these two loading modes.

In the MMT system, cells are encapsulated in microscale hydrogels in arrays of PDMS microwells that each contain two microcantilevers separated by 500 μm (**Figures 1**A–C). Arrays (10 × 13) of microwells were fabricated via replica molding.[19] A 100 μm diameter nickel sphere was adhered to one cantilever in each well to create a "magnetic pillar" for actuation and loading of individual microtissues (Figures 1A, B). Suspensions of NIH 3T3 fibroblasts and unpolymerized type-I collagen were centrifuged into the wells and the collagen was polymerized. The well surfaces were rendered non-adhesive to cells and collagen prior to seeding, and so, due to the contractile action of the cells on the collagen in each well, within a timescale of hours the cell/collagen construct contracted around the micropillars. This contraction led to the formation of aligned, dog-bone shaped microtissues suspended between the pillars that were prevented from slipping off the pillars by the pillars' heads (Figures 1B–D). The spontaneous contractile force F' within the microtissues deflected the pillars, causing displacements of the pillar heads observable via optical microscopy, which were used to calculate the contractile force according to cantilever bending theory.[19]

The microtissues were stable over the course of several days, with the cells remaining predominantly viable (Figure S3). **Figure 2**A shows 3D reconstructed views obtained with fluorescence confocal microscopy of F-actin (red), nuclei (blue) and collagen type I (green) of a microtissue section between the two pillars. Numerous thick F-actin stress fiber bundles aligned predominantly with the tissue contraction direction (x-axis) are visible. The nuclei were distributed densely within the collagen matrix and were elongated in the tissue contraction direction. These data suggested that the encapsulated cells were likely aligned with the tissue contraction direction, consistent with the expectation that contraction forces generated by the cytoskeletal networks of individual cells collectively provide the main sources of a microtissue's contraction force.

To apply external loading, we generated forces on the magnetic pillars of individual microtissues by applying an inhomogeneous magnetic field **B** with a magnetic tweezer.[20] The magnetic tweezer consisted of a computer-controlled electromagnet

Dr. R. Zhao, Dr. W.-G. Wang, Prof. D. H. Reich
Department of Physics and Astronomy
The Johns Hopkins University
3400 North Charles Street, Baltimore, MD, USA 21218
E-mail: reich@jhu.edu
Dr. T. Boudou, Prof. C. S. Chen
Department of Bioengineering
University of Pennsylvania
510 Skirkanich Hall, 210 South 33rd Street, Philadelphia, PA, USA 19104
E-mail: chrischen@seas.upenn.edu

DOI: 10.1002/adma.201203585

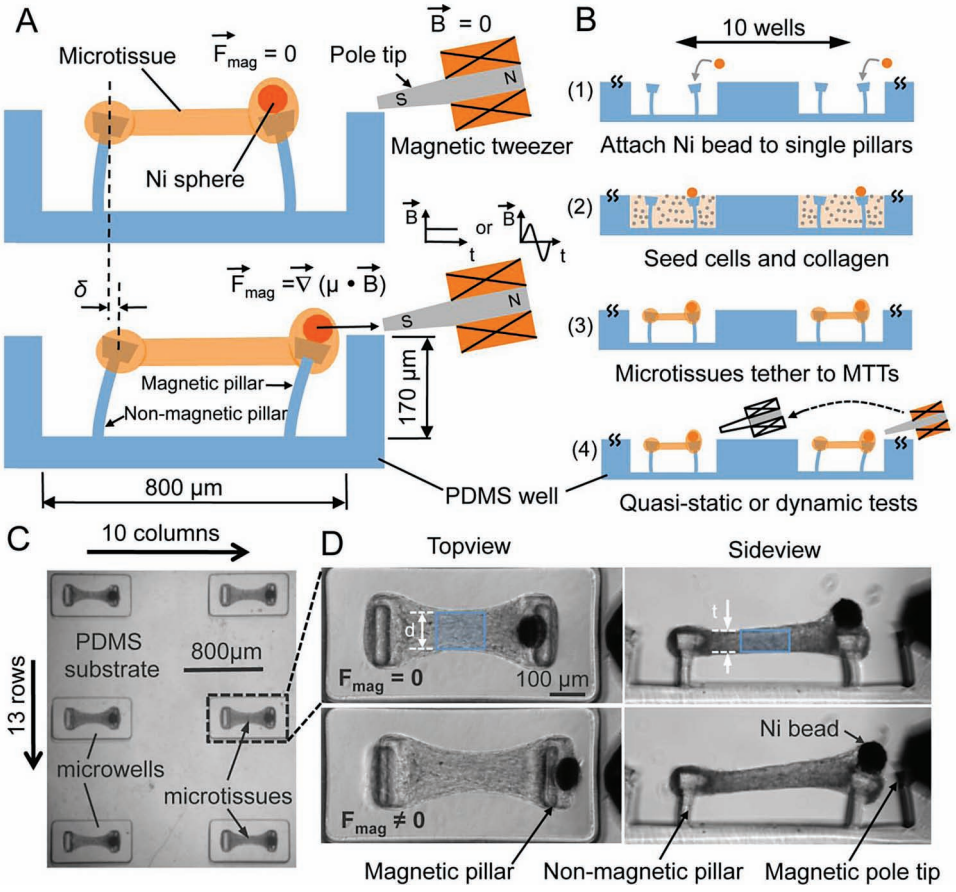

Figure 1. 3D microtissues tethered to magnetic microtissue testers (MMTs) to form an integrated culture system. (A) Schematic side-view of a microtissue being stretched by a MMT. The Ni sphere mounted magnetic pillar was driven by a magnetic force ($\mathbf{F}_{mag}$) under an applied magnetic field **B** produced by an electromagnetic tweezer. Tensile force ($\mathbf{F}_{tissue}$) in the microtissue was reported by the increased bending (δ) of the non-magnetic pillar. (B) Schematics show the fabrication, functionalization and operation of the system. (C) A portion of a large array (10 × 13) of microtissues tethered to MMTs. (D) Representative images depict a microtissue before ($\mathbf{F}_{mag} = 0$) and after ($\mathbf{F}_{mag} \neq 0$) magnetic force was applied. Shaded area indicates the central region used for tissue stiffness evaluation.

with a sharpened pole tip, which could be brought in close proximity to the Ni sphere (Figures 1A,D). Since the field magnetized the Ni sphere with a magnetic moment $\mu(\mathbf{B})$, the resulting force $\mathbf{F}_{Mag} = \nabla(\mu(\mathbf{B})\cdot\mathbf{B})$ was approximately quadratic with **B**, with some hysteresis, reflecting that of the sphere (Figure 2B). Magnetic forces up to ≈110 μN were generated to actuate the frame-like structure consisting of a microtissue tethered between two pillars (Figures 1A,D), and were sufficient to develop measurable strains in the microtissues and measurable movements of the pillar heads. The magnetic actuation system allowed versatility in loading control. In the current study, we applied both quasi-static tensile loading to measure the microtissues' stiffness and cyclic loading at 2 Hz to stimulate the microtissues dynamically (Figures 1A,B).

For quasi-static tensile tests, we displaced the magnetic pillar at a constant strain rate of approximately 0.09% s^{-1} in a step-wise ramp. The tension force applied to the microtissue was measured based on the deflection δ of the opposing non-magnetic pillar (Figure 1A). This force F increased with the field applied to the magnetic pillar and reached up to 15–30 μN depending on the stiffness of the tissue. At each loading step, the microtissue was allowed to stabilize for 2 s before images for force and strain measurements were taken. Visual checks confirmed that there was no creep in the microtissues during imaging. Also, no significant change was observed in the width d of the microtissues' cross-section during tensile tests (Figure 1D). The tensile stress of the microtissues was calculated as $\sigma = F/A$, where A is the cross-sectional area (Figure S2). The strain distribution in the central region of each microtissue, determined by a texture correlation algorithm (Figures 2C,D),[21] was relatively uniform (Figure 2E). The typical averaged strain ε over the central region in the tension direction could reach up to 10% before tensile failure, which occurred at the connections of the microtissue to the pillar heads. The resulting stress-strain curves were linear (Figure 2F), and the tissue elastic modulus was reported as the slope of these curves $E = d\sigma/d\varepsilon$. The tensile tests of the microtissues were performed in situ, thus avoiding perturbations that can arise from sample transferring, where loading of specimens is laborious and a major source of variability.[8,10,11]

To elucidate the cell and the collagen matrix contributions to the microtissues' mechanical properties, microtissues were

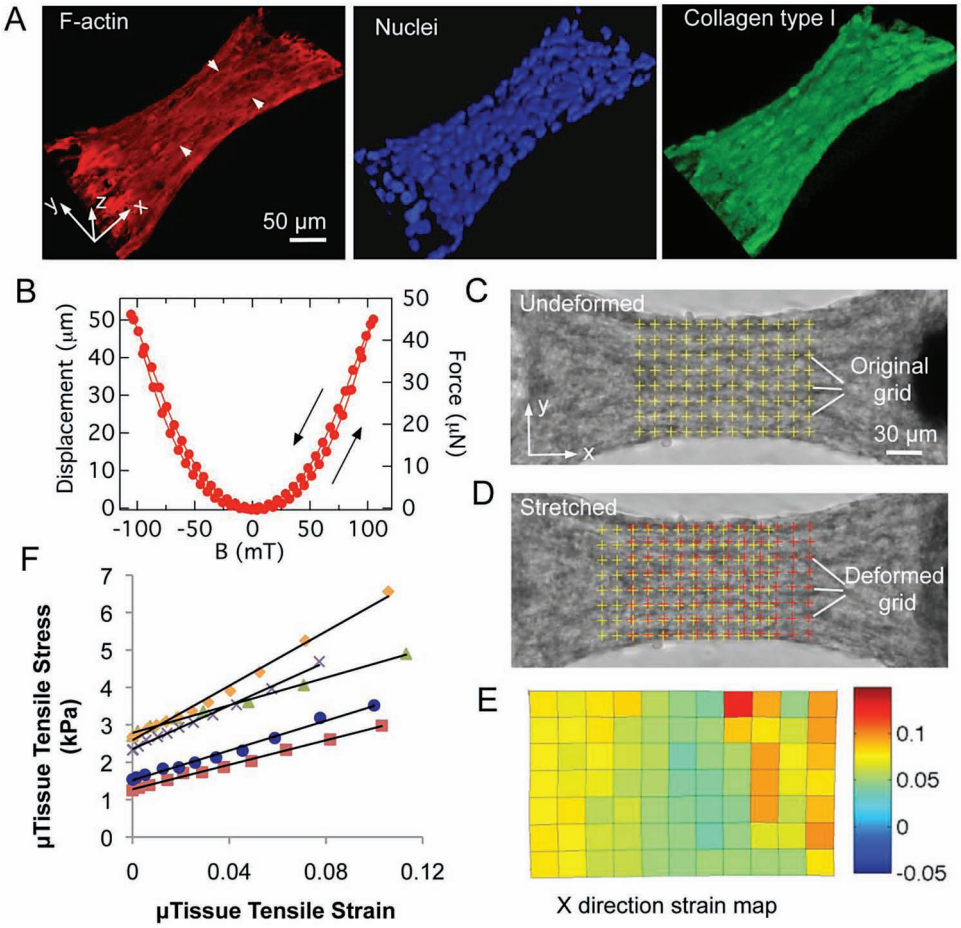

Figure 2. Microtissue structure, tensile testing and characterization of magnetic pillar actuation. (A) 3D reconstructed views of F-actin (red), nuclei (blue) and collagen type I (green) staining of a microtissue. Arrowheads show the F-actin stress fiber bundles. (B) Typical plot of single magnetic pillar displacement and force versus applied magnetic field **B** with no microtissue attached. Arrows indicate direction of the field change. Representative images depict the grid of nodes used in the texture correlation algorithm before (C) and after (D) stretch to determine strain. (E) X-direction strain map of the grid nodes shown in (D) corresponds to a 7% ± 3% averaged strain. (F) Representative stress-strain curves of microtissues. The tissue elastic modulus *E* is reported as the slope of such curves.

grown for 3 days and then given short pulse (≈20 min) treatments with blebbistatin – a myosin activity inhibitor,[22,23] Triton X-100 – a surfactant that permeabilizes the cellular membrane, trypsin/EDTA – an enzymatic compound that detaches cells from the extracellular matrix (ECM), or Latrunculin B (LatB) – an inhibitor for actin polymerization.[24] Blebbistatin caused little change in the tissue morphology and cell viability and some slight disruption of the F-actin stress fiber bundles (**Figures 3**A,B, and S3). Triton X significantly decreased the microtissues' cross sectional area (Figures 3A,B) and caused nearly complete cell death (Figure S3). LatB treatment caused slight decrease in the cross-sectional area and total disruption of the F-actin stress fibers, leading to F-actin aggregates visible in the microtissues (Figures 3A,B). Notably, nearly complete separation of cells from the matrix was achieved through trypsin/EDTA treatment, leaving an essentially bare collagen matrix behind (Figures 3A,B and S3). None of the biochemical treatments significantly disrupted the collagen matrix of the microtissues (Figure 3A). During these treatments we benefited from the small scale of the microtissues, which allowed fast diffusion of chemical factors and decellularization in seconds to minutes, and thus avoided prolonged biochemical treatments shown to adversely affect the intrinsic properties of the ECM (Figure S4).[25,26]

The cross-sectional stress $\sigma' = F'/A$ and the elastic modulus E of the microtissues were measured immediately after each biochemical treatment. Blebbistatin and LatB reduced the tissue contractile stress significantly (Figure 3B). The tissues' stress was reduced even more dramatically by Triton-X and trypsin treatment (Figure 3B), indicating that cellular forces were largely responsible for the measured tissue contraction forces. The presence of small residual stresses after killing (Triton X) or removing the cells (trypsin) showed that the collagen matrix was irreversibly compacted during tissue maturation, likely due to cross-linking of collagen fibrils by the cells.[27] Surprisingly, none of the treatments except for LatB caused significant change in the tissue elastic modulus (Figure 3C). In treatments that caused significant decrease in cross-sectional area (Triton-X and

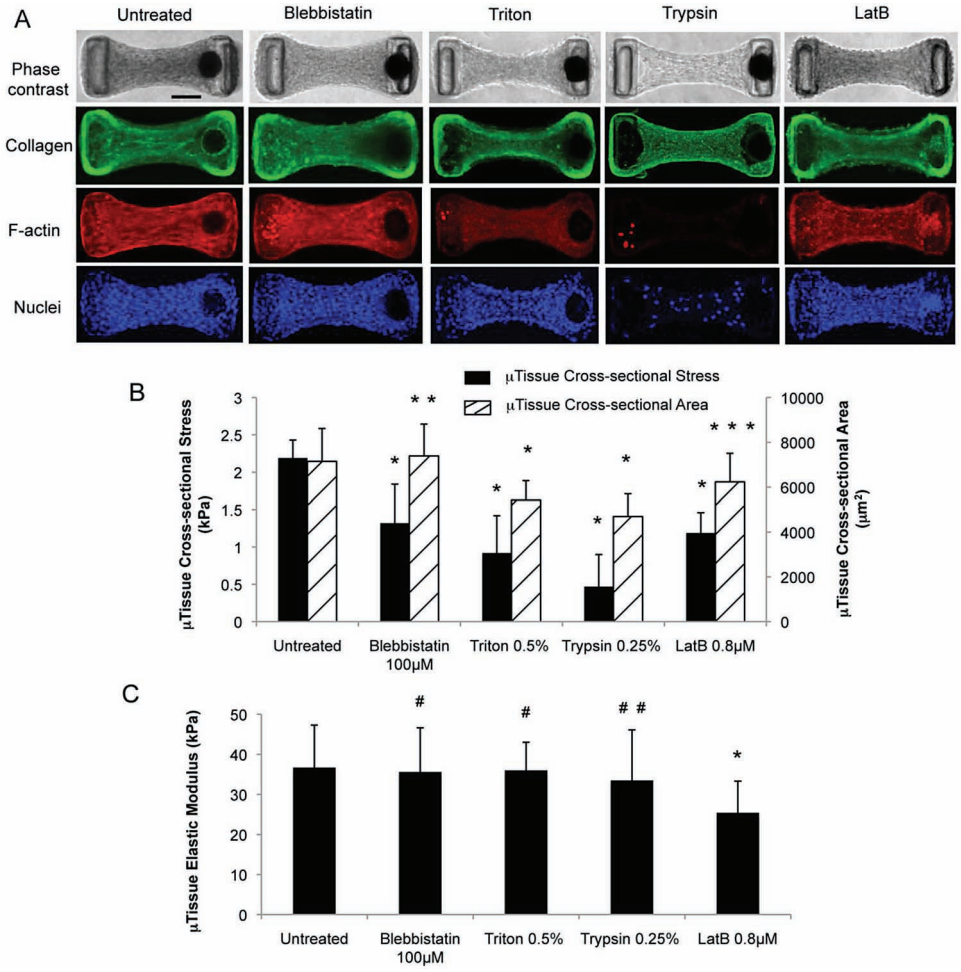

Figure 3. Cell and collagen matrix contributions to the microtissues' mechanical properties under static conditions. (A) Phase contrast images and 2D projected confocal images of collagen type I (green), F-actin (red) and nuclei (blue) of microtissues before and after short pulse pharmacological treatments. The bright dots in the red channel visible in the Triton and trypsin images are fluorescent beads used for displacement tracking. Comparisons of cross-sectional stress and cross-sectional area (B), and elastic modulus (C) of pharmacologically treated microtissues with those of untreated microtissues. *, $p < 0.003$; **, $p = 0.26$; ***, $p = 0.05$; #, $p > 0.35$; # #, $p = 0.17$ as compared to untreated condition by unpaired t-test. Scale bar = 100 μm. Sample sizes: untreated, n = 30; blebbistatin, n = 19; Triton, n = 20; trypsin, n = 14; LatB, n = 8. All data are presented as Mean ± S.D.

trypsin), we observed a proportional decrease in the microtissues' load bearing capacity F during tensile testing. As a result, the tensile stress σ was similar to that of the untreated samples. The strain level ε in such contractility-abolished tissues was also found to be similar to that of untreated tissues during tensile testing. Consequently, the elastic modulus E was unchanged following these treatments (Figures 3A–C). We also note that while both the blebbistatin and LatB treatments interfered with the cellular actomyosin force-generation machinery, and hence reduced the tissue stress levels, blebbistatin's impact on myosin activity likely led to little change in the load bearing capacity of the microtissues because the cells still contributed to the microtissue mechanics through the remaining actin cytoskeletal network (Figure 3A). Conversely, the disruption of the actin cytoskeletal network after LatB treatment disabled the cells' ability to contribute to the microtissues' load bearing capacity, and in conjunction with the minimal change in cross-sectional area, this led to the observed reduced elastic moduli (Figures 3A–C).

We then studied the cell and collagen matrix contributions to the microtissues' mechanical properties under dynamic mechanical stimuli. Microtissues were grown for 3 days and then subjected to cyclic stretch of 4% maximum strain at 2 Hz for 15 min., followed by either 58 min. recovery in normal culture conditions or 2.5 min. of short pulse treatment with Triton-X to eliminate the cell contribution. The microtissues' stiffness and dimensions were measured before, immediately after cyclic loading and 58 min. after cyclic loading, or after the Triton-X treatment. Comparison between phase-contrast images and fluorescent live cell images of the microtissues before and during stretch showed that encapsulated cells deformed with the collagen matrix as a coherent body and the mechanical stimulation was fully transferred to the cells (**Figure 4**A). All microtissues showed a sizable increase in elastic modulus (≈55%) (Figure 4B), a slight increase in length (≈2%) and a decrease in cross-sectional area (≈8%) immediately after cyclic stretch (Figures S5A,B). The microtissues' elastic modulus

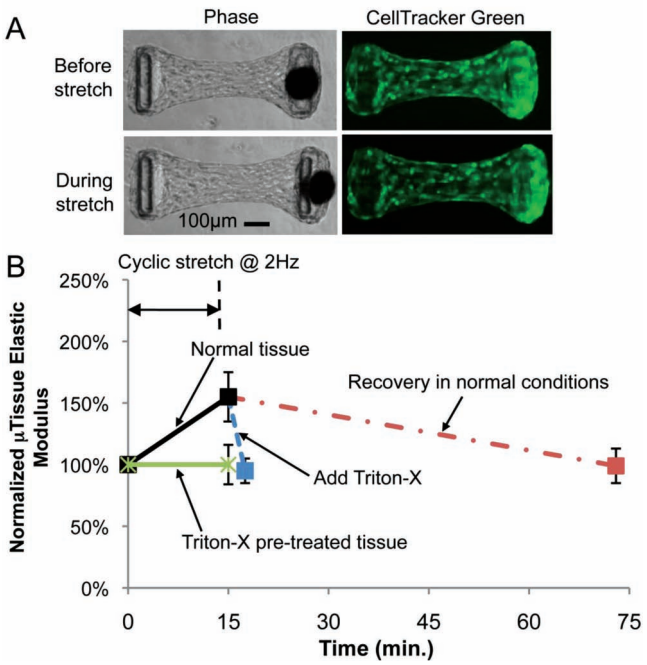

Figure 4. Cell and collagen matrix contributions to the microtissues' mechanical properties under dynamic loading. (A) Phase contrast and live cell labeled (CellTracker Green) images of microtissues before and during stretch. (B) Time course measurement of normalized microtissue elastic modulus. $p < 0.001$ between all experimental conditions and $p = 0.48$ between experimental conditions excluding increased elastic modulus of normal tissue by one-way ANOVA test. Sample sizes: normal tissue, n = 13; n = 6 for all other conditions. All data are presented as Mean ± S.D.

recovered to its original value (Figure 4B), and the length and cross-sectional area recovered by 1% and 4% respectively after 58 min. incubation in normal culture conditions (Figures S5A, B). For microtissues treated with Triton-X after cyclic loading, their elastic modulus dropped back to almost its original value (Figure 4B), the tissue length increased by 2%, and the cross-section area decreased by 5% after the treatment (Figures S5A, B). The return of the elastic modulus to its original value after both the spontaneous recovery and the Triton-X treatment indicated that mechanical activation of cells was likely responsible for the stiffening of the microtissues under cyclic loading since removal of the mechanically activated state of the cells through either recovery under static conditions or by compromising cellular integrity restored the original stiffness.

To separate further the cell and collagen matrix contributions to the microtissue stiffness under dynamic loading, we treated microtissues with Triton-X for 2.5 min. before any mechanical property measurement and then measured the tissue stiffness before and after 15 min. of cyclic loading at 2 Hz. We found there was no change in the microtissue stiffness before or after cyclic loading (Figure 4B). This absence of stiffness change showed that the collagen matrix alone does not respond to the cyclic loading, further confirming that the stiffness increase of the microtissues under cyclic loading was predominantly due to active changes in the cells. Similar to that observed in the live tissues, we found a slight (1%) increase in length for the Triton-X pre-treated microtissues after cyclic loading (Figures S5A,B). This indicates that the length change observed after dynamic loading is due to plastic deformation of the matrix, likely caused by straightening and aligning of the collagen fibrils during cyclic loading.

The above results offer several novel insights to the mechanics of engineered tissues. Cellular contractility and ECM stiffness have been identified as two central mechanical factors that regulate cell functions;[28,29] however, the relative contribution of these two mechanical parameters had not been examined simultaneously in 3D tissues. By introducing quasi-static external loading and transient biochemical treatments to the microtissues, notably, the removal of the cells with trypsin, which showed that the elastic modulus of the nearly bare collagen matrix was indistinguishable from that of the intact tissue, we were able to demonstrate that collagen matrix is the primary determinant of tissue stiffness, and the cells appear to adjust their own stiffness to match that of the matrix.[30,31] These experiments provide the first measurements that suggest that cellular contractility and matrix stiffness can be decoupled at the tissue level.

Dynamic loading has been shown by previous studies to enhance the stiffness of engineered tissues.[8,9] Here, the ability of our culture system to apply dynamic mechanical perturbations, transiently block cellular contributions, and simultaneously measure microtissue mechanical properties provides a novel approach to examine the mechanism for tissue stiffening under dynamic loading. Using this approach, we showed that cellular components rather than the matrix were the dominant contributors to the stiffness increase of the microtissues under cyclic loading, again decoupling the cell and matrix contributions to the microtissues' mechanical properties. This separation of cell and matrix contributions in both static and dynamic loading conditions showed that these two tissue components play different roles under these two loading modes. For example, while the collagen matrix mainly determined the tissue stiffness under static conditions, the tissue stiffness change was predominantly contributed by the cells under dynamic loading. This is likely because the cell-driven cross-linking of the matrix during tissue maturation provides a degree of irreversible mechanical stiffening to the collagen matrix,[27] so the increased tissue stiffness is maintained even after removal of cells. However, under short-term dynamic loading, cross-linking of the matrix had not yet occurred. Instead, it was the cells that were activated by the mechanical stimulation[11,32] and contributed to the stiffness increase.

Our culture system integrates magnetic actuation with arrays of microtissues to provide a novel platform for biomechanical studies of engineered tissues. This system allows fast biochemical assays, high-magnification microscopy, robust mechanical testing, and versatile dynamic stimulation of microtissues, and can perform all these tasks in situ and on large numbers of samples rapidly. Using this system, we decoupled the cell and collagen matrix contributions to the mechanical properties of microtissues in both static and dynamic loading conditions, shedding new light on the mechanics of engineered fibroblast-populated collagen tissues. Future studies can clearly be expanded to include other ECM compositions, and we anticipate that this system can be used to study the biomechanics of a broad variety of tissue types, and can also serve as a platform for rapid screening of drugs that target mechanically implicated pathologies, such as fibrosis and muscular degeneration.

Experimental Section

Fabrication of MMT Arrays: The MMT arrays (10 × 13) were cast from PDMS (Dow-Corning, Sylgard 184) via replica molding from masters made using a multilayer microlithography technique similar to that described previously.[19] The cured PDMS had an elastic modulus 1.6 MPa. The micropillars had an effective spring constant $k = 0.9\ \mu N\ \mu m^{-1}$. Nickel spheres for magnetic actuation (Alfa Aesar, CAS 7440–02–0, –150 + 200 mesh) and fluorescent latex microbeads 1 μm in diameter (L3030, Sigma) for displacement tracking were bonded using PDMS on top of the magnetic and non-magnetic pillars, respectively.

Microtissue Seeding and Cell Culture: Before cell seeding, the MMT arrays were sterilized in 70% ethanol for 15 min. and treated with 0.2% Pluronic F127 (BASF) for 7.5 min. to prevent cell adhesion. Unpolymerized rat tail collagen type I (BD Biosciences, 2.5 mg ml^{-1}) was mixed with NIH 3T3 fibroblasts and then introduced into the wells through centrifugation. Cell culture was maintained up to 3 days in high glucose DMEM containing 10% bovine serum, 100 units mL^{-1} penicillin, and 100 mg mL^{-1} streptomycin (all from Invitrogen), with the media changed after two days. The Ni concentration in the media due to dissolution from the Ni spheres after two days culture was 0.2 μM, as determined by inductively-coupled plasma mass spectrometry (ICP-MS), a level known to be biocompatible for in-vitro cell culture.[33–36]

Magnetic Characterization and Actuation: The tweezer's magnetic field was calibrated with a multilayer magnetic tunnel junction (MTJ) sensor.[37] During magnetic pillar actuation, changes in the magnetic field and image acquisition were synchronized under computer control. For cyclic loading, the tweezer was driven with a sinusoidal 1 Hz current, which generated loading at 2 Hz due to the quadratic response of the bead/tweezer system (Figure 2B).

Pharmacological Treatments of the Microtissues: To separate the cell and matrix contributions to tissue mechanical properties in static conditions, microtissues were grown for three days, and then treated with 100 μM blebbistatin (B0560, Sigma) for 20 min., 0.5% Triton X-100 for 20 min., 0.25% Trypsin-EDTA for 20 min. or 800 nM Latrunculin B (LatB, L5288, Sigma) for 20 min., followed by washing with phosphate buffered saline (PBS). For dynamic stimulation studies, 0.5% Triton X-100 was used to treat microtissues for 2.5 min. for various conditions.

Immunofluorescence and Microscopy: Collagen type I, F-actin, and cell nuclei were labeled using fluorescent staining and visualized via confocal microscopy. To measure contractile forces (pillar bending) and microtissue deformation, individual microtissues were imaged with a Nikon TE2000-E motorized microscope with a 10X objective.

Microtissue Stress and Strain Measurements: The microtissues were always under tension. Typical pillar deflections due to tissue contraction were 19 μm after 3 days culture, and this never decreased to less than ≈3 μm after either pharmacological treatment or mechanical conditioning. The spontaneous contraction force (or the residual force after biochemical treatment) $F' = k\delta'$ was determined from the average deflection δ' of the two pillars in the MMT, by comparing the deflected position of each pillar top with the location of its base. The cross-sectional stress was calculated as $\sigma' = F'/A$, where A is the cross sectional area of the center of the microtissue (Figure S2). The increasing force $F = k\delta$ in the microtissue during tensile testing was determined from the change in deflection δ of the non-magnetic pillar. The engineering stress of the microtissue during tensile testing was calculated as $\sigma = F/A$.

The strain ε over the central region of the microtissue was determined from the phase contrast images obtained during stretching, using a texture correlation algorithm.[21] Briefly, a grid of nodes with spacing $L = 9.6\ \mu m$ was assigned over the central region of the microtissue (Figure 2C), and the displacement of each node in the stretched images was tracked by examining the correlation of the intensity pattern surrounding the node in the stretched and unstretched configurations (Figure 2D). The engineering strain of each grid element along the stretching direction (Figure 2E) was calculated as $\varepsilon = \Delta L/L$, where ΔL is the distance change between two adjacent nodes. The average strain over the central region was calculated by averaging the strain of all grid elements in the region. The tissue elastic modulus $E = d\sigma/d\varepsilon$ was reported as the slope of the stress-strain curves.

Supporting Information

Supporting Information is available from the Wiley Online Library or from the author.

Acknowledgements

This work was supported in part by NIH grant HL90747. We thank J. Mihalic for assistance with ICP-MS measurements, which were performed at the Trace Metals Laboratory of the Johns Hopkins Bloomberg School of Public Health. VSM measurements and MTJ fabrication used facilities maintained by the Johns Hopkins Materials Research Science and Engineering Center. Confocal microscopy was performed at the JHU Integrated Imaging Center. ICP-MS analysis is supported in part by the Maryland Cigarette Restitution Fund Program at Johns Hopkins and the NIEHS Center P30 ES00319.

Received: August 28, 2012
Revised: November 5, 2012
Published online: January 28, 2013

[1] R. Langer, *Tissue Eng.* **2007**, *13*, 1.
[2] R. Langer, J. P. Vacanti, *Science* **1993**, *260*, 920.
[3] H. Vandenburgh, *Tissue Eng: Part B* **2010**, *16*, 55.
[4] D. L. Butler, S. A. Goldstein, F. Guilak, *J. Biomech. Eng.* **2000**, *122*, 570.
[5] R. M. Nerem, *Biorheology* **2003**, *40*, 281.
[6] F. J. Schoen, *Circulation* **2008**, *118*, 1864.
[7] M. Sacks, F. Schoen, J. Mayer, *Annu. Rev. Biomed. Eng.* **2009**, *11*, 289.
[8] S. Schutte, Z. Chen, K. G. Brockbank, R. M. Nerem, *Tissue Eng. Part. A* **2010**, *16*, 3149.
[9] Z. Syedain, R. Tranquillo, *Biomaterials* **2009**, *30*, 4078.
[10] J. P. Marquez, G. M. Genin, K. M. Pryse, E. L. Elson, *Ann. Biomed. Eng.* **2006**, *34*, 1475.
[11] A. Nekouzadeh, K. M. Pryse, E. L. Elson, G. M. Genin, *J. Biomech.* **2008**, *41*, 2964.
[12] A. Khademhosseini, R. Langer, J. Borenstein, J. P. Vacanti, *Proc. Natl. Acad. Sci. U S A* **2006**, *103*, 2480.
[13] P. Zorlutuna, N. Annabi, G. Camci-Unal, M. Nikkhah, J. Cha, J. Nichol, A. Manbachi, H. Bae, S. Chen, A. Khademhosseini, *Adv. Mater.* **2012**, *24*, 1782.
[14] A. P. Napolitano, P. Chai, D. M. Dean, J. R. Morgan, *Tissue Eng.* **2007**, *13*, 2087.
[15] G. M. Walker, H. Zeringue, D. J. Beebe, *Lab. Chip.* **2004**, *4*, 91.
[16] H. Aubin, J. Nichol, C. Hutson, H. Bae, A. Sieminski, D. Cropek, P. Akhyari, A. Khademhosseini, *Biomaterials* **2010**, *31*, 6941.
[17] S. Raghavan, C. Shen, R. Desai, N. Sniadecki, C. Nelson, C. Chen, *J. Cell. Sci.* **2010**, *123*, 2877.
[18] T. Boudou, W. R. Legant, A. Mu, M. A. Borochin, N. Thavandiran, M. Radisic, P. W. Zandstra, J. A. Epstein, K. B. Margulies, C. S. Chen, *Tissue Eng. Part. A* **2012**, *18*, 910.
[19] W. R. Legant, A. Pathak, M. T. Yang, V. S. Deshpande, R. M. McMeeking, C. S. Chen, *Proc. Nat. Acad. Sci. USA* **2009**, *106*, 10097.
[20] Y.-C. Lin, C. M. Kramer, C. S. Chen, D. H. Reich, *Nanotechnology* **2012**, *23*, 075101.

[21] R. Zhao, C. A. Simmons, *J. Biomech.* **2012**, *45*, 76.
[22] M. Kovács, J. Tóth, C. Hetényi, A. Málnási-Csizmadia, J. Sellers, *J. Biol. Chem.* **2004**, *279*, 35557.
[23] J. Limouze, A. Straight, T. Mitchison, J. Sellers, *J. Muscle. Res. Cell. Motil.* **2004**, *25*, 337.
[24] T. Wakatsuki, B. Schwab, N. C. Thompson, E. L. Elson, *J Cell Sci* **2000**, *114*, 1025.
[25] J. Liao, E. Joyce, M. Sacks, *Biomaterials* **2008**, *29*, 1065.
[26] P. M. Crapo, T. Gilbert, S. Badylak, *Biomaterials* **2011**, *32*, 3233.
[27] J. J. Tomasek, G. Gabbiani, B. Hinz, C. Chaponnier, R. A. Brown, *Nat. Rev. Mol. Cell. Biol.* **2002**, *3*, 349.
[28] D. E. Discher, P. Janmey, Y.-l. Wang, *Science* **2005**, *310*, 1139.
[29] B. Hinz, D. Mastrangelo, C. Iselin, C. Chaponnier, G. Gabbiani, *Am. J. Pathol.* **2001**, *159*, 1009.
[30] T. Yeung, P. C. Georges, L. A. Flanagan, B. Marg, M. Ortiz, M. Funaki, N. Zahir, W. Ming, V. Weaver, P. A. Janmey, *Cell. Motil. Cytoskeleton.* **2005**, *60*, 23.
[31] K. Ghosh, Z. Pan, E. Guan, S. Ge, Y. Liu, T. Nakamura, X. D. Ren, M. Rafailovich, R. A. Clark, *Biomaterials* **2007**, *28*, 671.
[32] S. Munevar, Y.-L. Wang, M. Dembo, *J. Cell. Sci.* **2004**, *117*, 85.
[33] J. Ryhanen, E. Niemi, W. Serlo, E. Niemela, P. Sandvik, H. Pernu, T. Salo, *J. Biomed. Mater. Res.* **1997**, *35*, 45.
[34] A. Hultgren, M. Tanase, C. S. Chen, G. J. Meyer, D. H. Reich, *J. Appl. Phys.* **2003**, *93*, 7554.
[35] A. Hultgren, M. Tanase, E. J. Felton, K. Bhadriraju, A. K. Salem, C. S. Chen, D. H. Reich, *Biotechnol. Prog.* **2005**, *21*, 509.
[36] M. Tanase, E. J. Felton, D. S. Gray, A. Hultgren, C. S. Chen, D. H. Reich, *Lab. Chip.* **2005**, *5*, 569.
[37] W. G. Wang, S. Hageman, M. G. Li, S. X. Huang, X. M. Kou, X. Fan, J. Q. Xiao, C. L. Chien, *Appl. Phys. Lett.* **2011**, *100*, 102502.